A lightweight three-phase Fluid Catalytic Cracking riser model for real-time simulation and interactive three-dimensional visualization

Florian de Vuyst, Laurent Desvillettes, Bruno Frogé, Jean-Michel Ghidaglia, Christophe Labourdette, Philippe Ricoux

A lightweight three-phase Fluid Catalytic Cracking riser model for real-time simulation and interactive three-dimensional visualization

Florian De Vuyst[a,*], Laurent Desvillettes[a], Bruno Frogé[b], Jean-Michel Ghidaglia[a], Christophe Labourdette[a], Philippe Ricoux[c]

[a] *CMLA UMR 8536, ENS Cachan, 61, Av. du Président Wilson, 94235 Cachan cedex France*
[b] *CEA, DAM, DIF, F-91297 Arpajon, France*
[c] *Total DG/DS, Tour Coupole, 2 Place Jean Millier, La Défense 6, 92078 Paris La Défense, France*

Abstract

In this paper, a lightweight physical model and a fast numerical solver are proposed for the rendering of fluid catalytic cracking (FCC) dynamics in the riser cylinder reactor part of the FCC unit. For Real Time requirements, a trade-off between the model fidelity and numerical complexity is needed. The choice of the physical model and the way to solve it numerically is here completely driven by the Real Time virtual reality requirements on a standard Personal Computer. It has been possible to design a real time numerical model able to show the three-phase flow dynamics depending on design parameters (number of oil injection inlets, injection angles, flow rates, temperature of cracking). The obtained flow is qualitatively in agreement with what is expected in such kind of reactive flows: expansion zones, recirculating zones for catalyst, turbulence, privileged paths for the gas phase, etc. Of course, the rendering is purely qualitative, but accurate enough to reproduce the emerging behaviors of the flow and roughly understand what happens in a riser reactor. This is of course important from the Engineering point of view. A Graphic User Interface (GUI) allows for near-Real Time (RT) user interaction on environmental parameters with instantaneous response of the flow. A VTK-based visualization module allows us to visualize the three-dimensional fields of the three phases, simultaneously or independently. The software was built with open source technologies including `Python`, `VTK`, `SWIG` for `C++` wrapping and `wxPython` and is portable over different operating systems like MS Windows and Linux. We think that this work is a new milestone toward a whole FCC unit closed-loop control simulator in the context of training and engineering. The perspective to use Teraflop-enabled Double Precision multicore GPU (see [9]) co-processors in the next months should allow us to use much more computational cells and particles, maybe up to a speedup factor of about 100 for a convincing realistic rendering. Moreover, the ability with such hardware to create software binding between data arrays and rendering objects with a high rate of frames per second is an attractive feature for real time visualization, simulation and interaction.

Keywords: Fluid catalytic cracking, riser, lightweight model, virtual reality, real time, numerical modeling, multiphase flow, particle method, three-dimensional visualization, VTK, GUI, interaction

1. Introduction

Fluid Catalytic Cracking (FCC) is one of the most important conversion processes used in petroleum refineries [2, 3, 4]. It is widely used to convert the high-boiling hydrocarbon fractions of petroleum crude oils to more valuable gasoline, olefinic gases and other products.

In recent designs, cracking takes place using a very active zeolite-based catalyst in a short-contact time vertical or upward sloped pipe called the "riser". Pre-heated feed is sprayed into the base of the riser via feed nozzles where it contacts extremely hot fluidized catalyst at 1200 to 1400°F (660 to 760°C). The hot catalyst vaporizes the feed and catalyzes the cracking reactions that break down the high molecular weight oil into lighter components including LPG, gasoline, and diesel. The catalyst-hydrocarbon mixture flows upward through the riser for just a few seconds and then the mixture is separated via cyclones. The catalyst-free hydrocarbons are routed to a main fractionator for separation into fuel gas, LPG, gasoline, naphtha, light cycle oils used in diesel and jet fuel, and heavy fuel oil.

During the trip into the riser, the cracking catalyst is "spent" by reactions which deposit coke on the catalyst and greatly reduce activity and selectivity. The "spent" catalyst is disengaged from the cracked hydrocarbon vapors and sent to a stripper where it is contacted with steam to remove hydrocarbons remaining in the catalyst pores. The "spent" catalyst then flows into a fluidized-bed regenerator where air (or in some cases air plus oxygen) is used to burn off the coke to restore catalyst activity and also provide the necessary heat for the next reaction cycle, cracking being an endothermic reaction. The "regenerated" catalyst then flows to the base of the riser, repeating the cycle. In FCC risers, multi-nozzle gas oil feed injectors are used for rapid feed vaporization and to enhance catalyst and oil uniform mixing and the finite mixing length at the bottom of the riser has a significant effect on the operation of FCC.

FCC units are clearly complex systems. Their numerical modeling is made difficult because of the highly complex Physics being involved (cracking chemical reactions, heat transfer, multiphase flows with phase change, turbulence phenomenon) but also because of the complex three dimensional geometry [5, 6, 7]. Today's dedicated CFD codes still require a few weeks of CPU time on a cluster of computers in order to obtain quantitatively acceptable results. Numerical computations are able to analyze the flow for a specific geometry and operating design.

Of course, it is of great industrial interest to come closer to real time numerical simulation of such kind of industrial process. Real time simulations with interactive user interface facilities can become simulators. Under real operating conditions, that can help for learning and understanding the whole system dynamics. Strongly accelerated computations also open for new ways of use like design of computer experiments (DoCE)

*Corresponding author

Email addresses: devuyst@cmla.ens-cachan.fr (Florian De Vuyst), laurent.desvillettes@cmla.ens-cachan.fr (Laurent Desvillettes), bruno.froge@cea.fr (Bruno Frogé), jmg@cmla.ens-cachan.fr (Jean-Michel Ghidaglia), labour@cmla.ens-cachan.fr (Christophe Labourdette), philippe.ricoux@total.com (Philippe Ricoux)

and exploration of the design space for optimal design and robustness assessment with respect to design uncertainties.

In this paper, we are interested in the design of a lightweight physical model able to capture some of the main flow features into the riser part of a FCC unit with capability to reach real time computations using convenient discretization techniques. We also address technical aspects like three dimensional dynamic visualization of solid-liquid-gas mixtures and graphical user interface issues.

Nomenclature

ε_{g}	gas phase volume fraction
ε_{s}	gas-solid emulsion phase void fraction
$\boldsymbol{g}$	gravity force m.s^{-2}
s_0	parameter in the pressure law
γ	gaseous phase heat capacity ratio
c	speed of sound
H	height of the riser reactor column (m)
z	coordinate in the vertical direction ($0 \leq z \leq H$)
$K_i,\ i = 1, \ldots 8$	some model constants
P	pressure
P_{s}	solid phase pressure
ρ_{g}	gas mean density (kg/m^3)
ρ_ℓ	liquid mean density (kg/m^3)
ρ_{s}	solid mean density (kg/m^3)
Γ_{g}	$= \log(\rho_g)$
r_ℓ	radius of the current liquid droplet (m)
R_ℓ	representativeness of the liquid droplet
R_{s}	representativeness of the solid macro-particle
$\bar{\bar{\tau}}_{\mathrm{g}}$	stress tensor for the gaseous phase
$\bar{\bar{\tau}}_{\mathrm{s}}$	stress tensor for the gas-solid emulsion phase
T	ambient temperature
$\boldsymbol{u}_{\mathrm{g}}$	gas mean velocity (m/s)
$\boldsymbol{u}_\ell$	liquid mean velocity (m/s)
$\boldsymbol{u}_{\mathrm{s}}$	solid mean velocity (m/s)
$\boldsymbol{v}_\ell$	liquid droplet velocity (m/s)
$\boldsymbol{v}_{\mathrm{s}}$	catalyst particle velocity (m/s)
$\boldsymbol{x}_\ell$	position of the current liquid droplet (m)
$\boldsymbol{x}_{\mathrm{s}}$	position of the current catalyst solid macroparticle (m)
q_g, q_{gv}, q_{gc}	terms modeling the expansion of the gas (kg/m^3)

2. State-of-the-art in FCC physical models

The hydrodynamics of FCC riser reactor has been studied with different modeling approaches. The accurate analysis of the flow field has not yet been achieved, and very often, it is limited to a two-dimensional flow description because of heavy CPU time requirements. The number of hydrocarbons chemical species being involved in cascade cracking reactions is of order 100. In most of the models found in the literature, only three or four lumps of chemical species are considered. This reduces the computational cost of course, but on the other hand the chemical model is harder to close because of difficulty to define reaction rates between the clusters.

Regarding the CFD model, the standard approach is to use a Euler-Euler two-phase gas-solid volume-averaged CFD model (see [1, 11, 8, 10, 12, 17] for example). The liquid crude oil entering the riser may be assumed to instantaneously vaporize at the contact of hot catalyst, creating a strong gas expansion. Balance equation are needed to describe the turbulent flow into the fluidized bed. Several approaches have been used in the past to simulate the fluidized bed. Krishna and van Baten [1] have proposed to use "pseudo-fluids" wherein the gas-solid emulsion phase and bubble phase are defined as two fluids. Physical properties are assumed for the emulsion phase, and empirical correlations are used to assess the velocity of the bubbles. The empirical parameters (like emulsion density, emulsion viscosity) need to be be fitted to match the experimental data. Hence, these models are not predictive in nature.

The continuity equation for the fluid phase is

$$\frac{\partial(\varepsilon_{\mathrm{g}}\rho_{\mathrm{g}})}{\partial t} + \nabla\cdot(\varepsilon_{\mathrm{g}}\rho_{\mathrm{g}}\boldsymbol{u}_{\mathrm{g}}) = 0. \tag{1}$$

Continuity equation for the emulsion phase is

$$\frac{\partial(\varepsilon_{\mathrm{s}}\rho_{\mathrm{s}})}{\partial t} + \nabla\cdot(\varepsilon_{\mathrm{s}}\rho_{\mathrm{s}}\boldsymbol{u}_{\mathrm{s}}) = 0. \tag{2}$$

Momentum equation for the fluid phase is

$$\frac{\partial(\varepsilon_{\mathrm{g}}\rho_{\mathrm{g}}\boldsymbol{u}_{\mathrm{g}})}{\partial t} + \nabla\cdot(\varepsilon_{\mathrm{g}}\rho_{\mathrm{g}}\boldsymbol{u}_{\mathrm{g}}\otimes\boldsymbol{u}_{\mathrm{g}}) = \tag{3}$$

$$\nabla\cdot\bar{\bar{\tau}}_{\mathrm{g}} + \varepsilon_{\mathrm{g}}\rho_{\mathrm{g}}\boldsymbol{g} - \varepsilon_{\mathrm{g}}\nabla P - \beta(\boldsymbol{u}_{\mathrm{g}} - \boldsymbol{u}_{\mathrm{s}}), \tag{4}$$

and momentum equation for the emulsion phase is

$$\frac{\partial(\varepsilon_{\mathrm{s}}\rho_{\mathrm{s}}\boldsymbol{u}_{\mathrm{s}})}{\partial t} + \nabla\cdot(\varepsilon_{\mathrm{s}}\rho_{\mathrm{s}}\boldsymbol{u}_{\mathrm{s}}\otimes\boldsymbol{u}_{\mathrm{s}}) = \tag{5}$$

$$\nabla\cdot\bar{\bar{\tau}}_{\mathrm{s}} + \varepsilon_{\mathrm{s}}\rho_{\mathrm{s}}\boldsymbol{g} - \nabla\cdot P_{\mathrm{s}} - \varepsilon_{\mathrm{s}}\nabla P + \beta(\boldsymbol{u}_{\mathrm{g}} - \boldsymbol{u}_{\mathrm{s}}). \tag{6}$$

In the volume-averaged momentum equations, we find the inertial terms, the stress forces, the gravity force, the pressure forces and the drag forces between the two phases. As usual, the stress tensors are defined from their diagonal and deviatoric parts and the Lamé coefficients λ and μ. For $i = \mathrm{g}, \mathrm{s}$, we have

$$\bar{\bar{\tau}}_i = 2\mu_i\bar{\bar{D}}_i + \left(\lambda_i - \frac{2}{3}\mu_i\right)\cdot tr(\bar{\bar{D}}_i)\bar{\bar{I}}, \tag{7}$$

with

$$\bar{\bar{D}}_i = \frac{1}{2}\left[\nabla \boldsymbol{u}_i + (\nabla \boldsymbol{u}_i)^T\right]. \tag{8}$$

To these equations, we also should add energy or heat balance equations, because the temperature is an important variable that drives the chemical reaction rates. The discretization of this system of equations is a difficult task that requires expertise in computational physics and numerical analysis. Generally, the time advance schemes are subject to some time step constraints because of numerical stability requirements. That makes the numerical simulation very time consuming, and in particular very far from real time simulation for reasonable spatial meshing. The discretization of these equations is not in the scope of this paper. We rather look for relevant simplifications of the equations with suitable fast solvers.

In order to strongly lower the computational complexity, one can think about a change of modeling paradigm while trying to reproduce the expected emerging behaviours and features. There is interesting emerging literature and ongoing research about this topic [14, 15, 16]. For example, Pannala et al. [15] in 2003 proposed a new paradigm of description of the flows into reacting bubbling beds using agent-based bubble models. They propose a low-order dynamical model that includes mass-transfer and first-order reactions between the gas and solids and accounts for upward motion and interactions betweens bubbles, thus creating a large scale discrete dynamical system. The collective result of the bubble dynamics provides a global emergent behavior characterized by the formation of a pulsing central channel of high void fraction and high gas flow. After parameter identification, on a time-average axis they get reasonably good agreement between the model and experimental measurements. In [16], the authors claim that this kind of low-order model allows for near real-time simulation of large fluidized beds. Of course, as in [1] the empirical parameters need to be be fitted to match the experimental data. Hence, these models are not predictive in nature.

The original pioneer works by Pannala et al. let us think that low-order models should be much more considered for the numerical simulation of fluidized beds and that there are certainly many ways to lower the scale of these problems or equations with suitable dedicated solvers.

3. Functional requirements

Our simplified lightweight models will be designed according to the following functional requirements:

1. The model must include all the phases being present into the riser reactor, namely the particle solid catalyst, the liquid crude oil and hydrocarbons and water steam in gaseous state.
2. The turbulence into the fluidized bed which is an important feature of the flow must be rendered.
3. The numerical model must be able to capture some expected flow features and emerging behaviours like strong gas expansion near crude oil injection, recirculating patterns for catalyst solid phase [11], privileged paths for gas phase (well formation into the catalyst bed) [11], strong turbulence in bottom

part of the riser column, laminar regime in the top part, fall down of particles near the riser cylinder by gravity forces.

4. According to their residence time into the riser reactor, catalyst particles lose their efficiency because of the deposition of coke by cracking reactions. The model should take this feature into account, and the level of catalyst powder fouling should be visualized.
5. The numerical model should allow for real-time, or near real-time simulation on a standard workstation or a powerful laptop.
6. The visualization component should allow for three-dimensional dynamical visualization and be able to provide the simultaneous rendering of the solid, liquid and gaseous phases. The standard PC will be assumed to have 3D graphic hardware acceleration and OpenGL support.
7. The user should be able to dynamically interact with the system during runtime simulation. Parameters like crude oil inflow or the inlet attack angles can be modified by the user during simulation in order to assess the sensitivity of the flow with respect to some design parameters.

4. Strategy to reach 3D Real Time interactive simulation

By Real Time, it is understood that the time clock of the simulation runs at physical time. Ideally, time steps should be less than 1/25 second in order to get a sampling quality of the order of a film or video. The Finite Volume discretization of Euler-Euler volume averaged multiphase models is known to be very time consuming even for explicit schemes where the time step is strongly limited because of restrictive CFL number stability conditions. Implicit Eulerian schemes are not feasible candidates for Real Time requirement. We then have to think about another description of the fluid flow, as in Pannala and coworkers [15]. The use of Lagrangian models and computational approaches, at least for the liquid and solid phases appears to be an interesting option. The solid catalyst powder will be considered as a system of macro-particles that interact between themselves but also with the liquid droplets and the surrounding gaseous phase. The liquid phase is weakly present in the riser reactor. Indeed, the liquid crude oil entering at the inlets is rapidly vaporized by contact with the catalyst particles. In the contact region, there are strong gas expansions due to the liquid-to-gas phase change. The flow is turbulent in this region, it is reasonable to think that the liquid jet here breaks into small droplets. We will then consider the liquid phase as a systems of spherical droplets with variable diameters. The droplet diameters themselves will be unknown variables. Some differential equations will govern the decay of the diameters in time according to the rate of phase change.

Another approximation consists in considering liquid as well as solid phases as dispersed phases into the gas phase. In that case, the gaseous phase can be represented with an Eulerian monophasic model including sources terms for phase changes. Another difficulty is the discretization of viscous terms that generally requires implicit schemes because of the too much restrictive CFL conditions of explicit schemes. For that

reason, the gaseous phase will be considered as inviscid. Regarding the solid and liquid phases, the diffusion will be treated through its microscopic interpretation using a stochastic diffusion process. It is made possible by the Lagrangian description. The equations of motion will then be formulated as stochastic differential equations using a stochastic Wiener process in order to represent the fluctuations of the velocity field.

Because of strong changes of volume of gas due to the phase change of liquid into gas, it appears necessary to consider the gaseous phase as a compressible fluid. The inviscid compressible gaseous phase will then be modeled by the compressible Euler equations. Such equations are hyperbolic and finite volume solvers need artificial viscosity to be stable. Usually the artificial viscosity comes from an upwind discretization strategy. Even for one-phase fluids, in a simple three-dimensional geometry like a cylinder, today's personal computers are still not powerful enough for Real Time (except using very coarse grids). We have to add computational tricks to reach near Real Time. We adopted an embedded approach where the cylinder is embedded into a squared-base cylinder, allowing us to deal with cartesian grids first, then to apply an alternate directions fractional step method strategy in order to lower the computational complexity. This approach is also suitable for parallel computing on a multicore architecture. This will be detailed and discussed later.

Because of today's limited computing power, it still seems impossible to consider convection-diffusion-reaction equations for the different hydrocarbons chemical species. Even with a lump strategies involving a low number L of chemical lumps, the chemistry component would require the solution of L additional partial differential equations. What we propose here to do is to skip the chemistry and to consider the gas phase as the mixture of the different vaporized hydrocarbons. In some sense, the liquid-gas phase transition law (involving important volume ratios and gas expansion) in our model captures the important feature of the chemistry that mainly acts on the flow dynamics. What could perhaps be possible is to include an indicator of fraction of cracked hydrocarbons.

We summarize the retained choices and assumptions for the FCC riser lightweight physical and numerical model:

- solid and liquid phases are seen as dispersed phases into the solid-gas emulsion gaseous phase;
- the particle solid phase model will be set in Lagrangian form and represented by a set of macro-particles. Ordinary differential equations of motion will be used;
- the hydrocarbon liquid phase will be set in Lagrangian form and represented by a set of spherical droplets of varying radius. Ordinary differential equations for the motion and evolution of the radius will be used;
- the leading solid-gas emulsion gaseous phase will be considered as an inviscid compressible gas and will be set in Eulerian form. A three dimensional fast Euler solver is needed for the numerical discretization;

- for coupling the different models, macroscopic quantities defined into fixed Eulerian cells will be defined. In particular for solid and liquid phases, particles representativeness will be used for definition of macroscopic quantities (like densities or momentum)
- there is no chemical model;
- the empirical phase change source terms will depend on macroscopic densities and the ambient temperature, considered as a constant parameter in the model.

5. Solid phase catalyst modeling

5.1. Physical model

The solid catalyst powder phase is seen as a dispersed phase within the gaseous phase. It is described by particles obeying the following ordinary differential equations of motion (we denote by $\boldsymbol{x}_\mathrm{s} = (x_s, y_s, z_s)$ and $\boldsymbol{v}_\mathrm{s}$ the position and velocity of those particles, we also denote $\boldsymbol{z} = (0, 0, z_s)$):

$$\dot{\boldsymbol{x}_\mathrm{s}} = \boldsymbol{v}_\mathrm{s}, \tag{9}$$

$$\dot{\boldsymbol{v}_\mathrm{s}} = K_1\,\rho_\mathrm{g}\,(\boldsymbol{u}_\mathrm{g} - \boldsymbol{v}_\mathrm{s} + 2\,(1 - \frac{z_s}{H})^2\,(\boldsymbol{v}_\mathrm{s})_z\,\boldsymbol{z_s}) + K_2\,\rho_\ell\,(\boldsymbol{u}_\ell - \boldsymbol{v}_\mathrm{s}) + \boldsymbol{g}. \tag{10}$$

In the acceleration, there is a drag force between gas and solid phase proportional to $\boldsymbol{u}_\mathrm{g} - \boldsymbol{v}_\mathrm{s}$, a drag force between liquid and solid phase proportional to $\boldsymbol{u}_\ell - \boldsymbol{v}_\mathrm{s}$, an added mass term proportional to $(\boldsymbol{v}_\mathrm{s})_z$ and the gravity force $\boldsymbol{g}$. Those equations are complemented with the following boundary conditions:

- rebound on the lateral wall of the cylinder with Descartes' law with respect to the two horizontal coordinates x and y; the vertical velocity is set to 0 in order to take into account the boundary layer;
- the particles coming out of the cylinder are reintroduced at its basis with a velocity with an upward orientation.

5.2. Numerical model, coupling with liquid and gas models

The differential equations (9), (10) are discretized thanks to the implicit first order Euler method.

There is some interaction with the liquid and gaseous phases thanks to the macroscopic quantities $\boldsymbol{u}_\ell$, ρ_g and $\boldsymbol{u}_\mathrm{g}$. As we will see later, these quantities are defined on fixed Eulerian cells. Considering the particles $\boldsymbol{x}_\mathrm{s}$, we have to find the Eulerian cell $\mathscr{C}$ that contains $\boldsymbol{x}_\mathrm{s}$.

As an output for the liquid phase and gas phase models, we have to compute some macroscopic solid densities and mean velocities into the fixed Eulerian cells from the computed positions and velocities of solid particles. Each particle has a representativity R_s that gives a correspondence between the number of

macro-particles and the actual solid density (that is, the mass of each macro-particle is $\frac{4}{3}\,\pi\,R_s$). In a given Eulerian cell, the macroscopic quantities $\rho_{\rm s}$ and $\boldsymbol{u}_{\rm s}$ are then computed according to the formulas

$$\rho_{\rm s} = R_{\rm s}\,\frac{4}{3}\,\pi\,\frac{1}{vol(\text{Eulerian cell})}\sum_{\boldsymbol{x}_i\in\text{ Eulerian cell}} 1,$$

$$\rho_{\rm s}\,\boldsymbol{u}_{\rm s} = R_{\rm s}\,\frac{4}{3}\,\pi\,\frac{1}{vol(\text{Eulerian cell})}\sum_{\boldsymbol{x}_i\in\text{ Eulerian cell}} (\boldsymbol{v}_i)_{\rm s},$$

The rebound on the wall of the cylinder is computed exactly except for (the very rare) particles which touch two times the wall during a time step.

6. Liquid phase modeling

6.1. Physical model

The liquid phase is assumed to be dispersed within the surrounding gaseous phase. As discussed, the liquid phase is represented as a set of droplets of variable radius. Each droplet is described by a particle ℓ obeying the following set of ordinary differential equations (we denote by $\boldsymbol{x}_\ell$ and $\boldsymbol{v}_\ell$ the position and velocity and by r_ℓ the radius):

$$\dot{\boldsymbol{x}_\ell} = \boldsymbol{v}_\ell, \tag{11}$$

$$\dot{\boldsymbol{v}_\ell} = K_3\,\rho_{\rm s}\,(\boldsymbol{u}_{\rm s} - \boldsymbol{v}_\ell) + \mathbf{g}, \tag{12}$$

$$\dot{r_\ell} = -(K_4 + \rho_{\rm s})\,(K_5 + T)\,r_\ell. \tag{13}$$

Expressions (11),(12) are the equations of motion. The acceleration is made of a drag term between liquid and solid phases and the gravity term. The third equation (13) governs the evolution of the droplet radius. The decay rate depends on the solid mean density and the ambient temperature.

The following boundary conditions are added to these equations:

- rebound with Descartes' law on the lateral wall and the basis of the cylinder;
- elimination of the particles at the top of the cylinder and when the radius becomes less than a given threshold;
- introduction of new particles at the inlets with a given law (for example a velocity law) at specified points.

6.2. Numerical model

As for the solid phase, the differential equations (11) – (13) are discretized thanks to the simple implicit (first order) Euler method. The macroscopic mean quantities $\rho_{\rm s}$ and $\boldsymbol{u}_{\rm s}$ are those of the cell containing $\boldsymbol{x}_{\rm s}$.

The boundary conditions are discretized in the same way as for the solid particles, except that the positions, velocities and radiuses of liquid particles emitted are computed thanks to a random process controlled by the user.

As an output of the liquid phase model, the macroscopic quantities mean density ρ_ℓ and mean liquid velocity $\boldsymbol{u}_\ell$ are computed according to formulas in which each particle has a representativity R_ℓ that gives a correspondence between the number of macro-particles and the actual liquid density (that is, the mass of each macro-particle of radius r_ℓ is $\frac{4}{3}\,\pi\,R_\ell\,r_\ell^3$):

$$\rho_\ell = R_\ell\,\frac{4}{3}\,\pi\,\frac{1}{vol(\text{Eulerian cell})}\sum_{\boldsymbol{x}_i\in\text{Eulerian cell}}(r_i)_\ell^3,$$

$$\rho_\ell\,\boldsymbol{u}_\ell = R_\ell\,\frac{4}{3}\,\pi\,\frac{1}{vol(\text{Eulerian cell})}\sum_{\boldsymbol{x}_i\in\text{Eulerian cell}}(r_i)_\ell^3\,(\boldsymbol{u}_i)_\ell.$$

7. Gaseous phase modeling

7.1. Physical model

Viscous effects of the gaseous phase are first neglected. The model is expected to capture the gas expansion due to cracking and vaporization effects near oil feed injectors. So it is necessary to consider the gaseous phase as a compressible fluid with density $\rho_{\rm g}$. For the sake of computational performance, the gas phase is considered here as a perfect gas with isentropic index γ equal to 1.4, even if, of course, this is not realistic. Heat effects will be only modeled by means of empirical source terms, so that the energy balance equation will be skipped and the evolution gaseous phase will be assumed to be isentropic with an equation of state of the form

$$P = s_0\,\rho_{\rm g}^\gamma \tag{14}$$

with a constant s_0. The continuity equation

$$\partial_t\rho_{\rm g} + \nabla\cdot(\rho_{\rm g}\boldsymbol{u}_{\rm g}) = q_g, \tag{15}$$

expresses the mass balance equation with gas velocity $\boldsymbol{u}_{\rm g}$ and a gas source term q_g which consists of two contributing source terms:

$$q_g = q_{g,v} + q_{g,c}. \tag{16}$$

The source term $q_{g,v} \geq 0$ expresses the mass transfer from the liquid phase to the gaseous phase by heating. The source term $q_{g,c} \geq 0$ takes into account the gas volume expansion due to the molecular cracking. The

liquid-to-gas phase change term

$$q_{g,v} = K_8\,\rho_\ell \tag{17}$$

is empirically imposed. For $q_{g,c}$, the following empirical law is used:

$$q_{g,c} = \rho_g\, f(\rho_s, T, z) \tag{18}$$

with

$$f(\rho_s, T, z) = (K_6\,\rho_s + K_7\,T)\left(1 - \frac{z}{H}\right),\ 0 \le z \le H \tag{19}$$

where K_6 and K_7 are two positive constants. In (19), it is assumed that there is no more hydrocarbon cracking at the riser top. The gas production is assumed to be proportional to the solid density and the reactor temperature. Notice that

$$\partial_{\rho_s} f = K_6\,(1 - \frac{z}{H}) \ge 0,\ \partial_T f = K_7\,(1 - \frac{z}{H}) \ge 0,$$

and

$$\partial_z f = -\frac{1}{H}\,(K_6\,\rho_{\rm s} + K_7\,T) \le 0,$$

so we have the expected evolution directions according to the solid density $\rho_{\rm s}$, riser temperature T and column height z.

Now let us consider the momentum balance equation. It reads

$$\partial_t(\rho_g \boldsymbol{u}_{\rm g}) + \nabla\cdot(\rho_{\rm g}\boldsymbol{u}_{\rm g}\otimes\boldsymbol{u}_{\rm g}) + \nabla P = \rho_{\rm g}\,\boldsymbol{g} + q_g\,\boldsymbol{u}_\ell. \tag{20}$$

Notice that the force term $(q_g\boldsymbol{u}_\ell)$ due to gas production q_g is obtained by a multiplication with the liquid velocity $\boldsymbol{u}_\ell$. It seems natural to consider the liquid velocity there (near the crude oil feed injectors) because the gas (which just vaporized) was previously travelling with the velocity of the liquid phase. Far from feed injectors, anyway $\boldsymbol{u}_\ell$, $\boldsymbol{u}_{\rm g}$ and $\boldsymbol{u}_{\rm s}$ are quite close because of drag forces that act as homogeneous velocity relaxation terms.

We close this subsection by briefly listing the values of the constants K_i used above, namely $K_1 = 100.0$, $K_2 = 100.0$, $K_3 = 200.0$, $K_4 = 0.01$, $K_5 = 200.0$, $K_6 = 1000.0$, $K_7 = 0.01$, $K_8 = 50.0$. Those constants are not extracted from physical experiments. They are introduced for providing a good visual rendering (that is, qualitatively close to what is observed in real experiments) of the results of the code, and sometimes for avoiding singularities when some of the parameters are close to the limit of their range (this is the case for K_4 and K_5).

7.2. Computational approach and numerical modeling

We are looking for a fast solver of the time-dependent compressible Euler equations in a three dimensional cylinder domain. The Euler equations are hyperbolic equations so we have to take care of the discretization

of the equations including upwinding and/or artificial viscosity for numerical stability purposes. Introducing the gaseous particle derivative

$$D_t = \frac{\partial}{\partial t} + \boldsymbol{u}_{\rm g} \cdot \nabla, \tag{21}$$

the gaseous phase continuity equation can be written

$$D_t\, \rho_{\rm g} + \rho_g \nabla \cdot \boldsymbol{u}_{\rm g} = q_g,$$

and the momentum equation can be written as

$$D_t\, \boldsymbol{u}_{\rm g} + \frac{1}{\rho_{\rm g}} \nabla p(\rho_{\rm g}) = \boldsymbol{g} + \frac{q_g}{\rho_{\rm g}} \boldsymbol{u}_\ell.$$

By introducing the new variable

$$\Gamma_{\rm g} = \log(\rho_{\rm g}), \tag{22}$$

the isentropic Euler system can be written as

$$D_t\, \Gamma_{\rm g} + \nabla \cdot \boldsymbol{u}_{\rm g} = \exp(-\Gamma_{\rm g})\, q_g, \tag{23}$$

$$D_t\, \boldsymbol{u}_{\rm g} + \nabla q(\Gamma_{\rm g}) = \boldsymbol{g} + q_g \exp(-\Gamma_{\rm g}) \boldsymbol{u}_\ell, \tag{24}$$

with

$$q(\Gamma_{\rm g}) = \frac{\gamma}{\gamma - 1}\, s_0\, \exp((\gamma - 1)\, \Gamma_{\rm g}),$$

where we used particle derivatives into the Euler system (23),(24). Material waves at velocity $\boldsymbol{u}_{\rm g}$, acoustic pressure waves due to compressibility (term $\nabla \cdot \boldsymbol{u}_{\rm g}$) and elastic pressure response are separated. A simple way to solve this system is to use a fractional step method where material waves are first solved by means of a simple transport equation solver, then acoustic pressure waves are considered. The fractional step approach also allows for a separate treatment of the source terms.

For computational efficiency, the numerical discretization of the system is performed on a cartesian grid $\mathscr{G}$ indexed by triplets (i, j, k). Is is assumed that the riser reactor cylinder is embedded into a square-base cylinder S and that S is meshed by $\mathscr{G}$. In what follows, any discrete variable $X_{i,j\,,k}$ will denote the quantity X at coordinates (x_i, y_j, z_k), $x_i = i\, h_x$, $y_j = j\, h_y$, $z_k = k\, h_z$, $i = -N_x/2, \ldots, N_x/2$, $j = -N_y/2, \ldots, N_y/2$, $k = 0, \ldots, N_z$.

The fast numerical solver will be designed as follows:

1. Lagrangian derivatives will be integrated by a semi-lagrangian approach;
2. For the other terms, especially for extra fluxes, the simple robust Rusanov method will be used. This numerical scheme naturally introduces artificial viscosity in an easy way and does not require any eigen-decomposition of the system.

3. As an additional simplification, an alternate direction (AD) integration fractional step method will be used. This computational approach allows us to sequentially treat the equations as one-dimensional ones, thus leading to very simple schemes to write and to compute. In particular, the semi-Lagrangian part becomes very simple to implement.

We shall now go into details of the implementation of the fractional step method during a time step Δt.

7.2.1. Numerical integration of the mass source term

On each computational cell (i, j, k), the following system

$$\partial_t \, \Gamma_{\rm g} = \exp(-\Gamma_{\rm g}) \, q_g,$$
$$\partial_t \, \boldsymbol{u}_{\rm g} = 0,$$

is time integrated over a time step Δt. Using the first order Euler scheme, this gives

$$(\Gamma_{\rm g})_{i,j\,,k} \leftarrow (\Gamma_{\rm g})_{i,j\,,k} + \Delta t \, \exp(-(\Gamma_{\rm g})_{i,j\,,k}) \, (q_g)_{i,j\,,k}$$

with $\boldsymbol{u}_{\rm g}$ unchanged.

7.2.2. Integration step in the direction x

Denoting by u, v, w the three components of the velocity vector, i.e. $\boldsymbol{u}_{\rm g} = (u_{\rm g}, v_{\rm g}, w_{\rm g})$, $\boldsymbol{u}_\ell = (u_\ell, v_\ell, w_\ell)$, this step corresponds to the integration over a time step Δt of the system

$$D_t^x \Gamma_{\rm g} + \partial_x u_{\rm g} = 0,$$
$$D_t^x u_{\rm g} + \partial_x (q(\Gamma_{\rm g})) = q_g \exp(-\Gamma_{\rm g}) u_\ell,$$
$$D_t^x v_{\rm g} = 0,$$
$$D_t^x w_{\rm g} = 0,$$

where the operator D_t^x denotes

$$D_t^x = \frac{\partial}{\partial t} + u_{\rm g} \, \frac{\partial}{\partial x}.$$

This system may be written in vector conservation form

$$D_t^x \, \mathbf{U} + \partial_x \, \mathbf{F} = \mathbf{S}_x.$$

For the integration of the Lagrangian derivative, we use a one-dimensional method of characteristics. The fields $\Gamma_{\rm g}$, $u_{\rm g}$, $v_{\rm g}$ and $w_{\rm g}$ are reconstructed by linear interpolation between two consecutive grid points (i, j, k) and $(i + 1, j, k)$.

For the discretization of the partial derivative $\partial_x \mathbf{F}$, we use a conservative Finite Volume approach with a Rusanov numerical flux. The speed of pressure waves is the speed of sound c defined by

$$c^2 = \frac{dP}{d\rho} = \frac{\gamma P(\rho)}{\rho}.$$

This approach gives the following time advance scheme:

$$\begin{aligned}
\boldsymbol{U}_{i,j\,,k} \leftarrow & \left(1 - \frac{\Delta t}{h_x}(u_{\mathrm{g}})_{i,j\,,k}\right) \boldsymbol{U}_{i,j\,,k} \\
& + \frac{\Delta t}{h_x} \max(0, (u_{\mathrm{g}})_{i,j\,,k})\, \boldsymbol{U}_{i-1,j\,,k} \\
& + \frac{\Delta t}{h_x} \min(0, (u_{\mathrm{g}})_{i,j\,,k})\, \boldsymbol{U}_{i+1,j\,,k} \\
& - \frac{\Delta t}{h_x} \left(\Phi_{i+1/2,j,k} - \Phi_{i-1/2,j\,,k}\right) + \Delta t\, (\boldsymbol{S}_x)_{i,j\,,k},
\end{aligned}$$

with a numerical flux written in viscous form, i.e. with a center flux plus an artificial viscosity term

$$\Phi_{i+1/2,j,k} = \frac{\boldsymbol{F}_{i,j\,,k} + \boldsymbol{F}_{i+1,j,k}}{2} - \frac{1}{2} \max(c_{i,j\,,k},\, c_{i+1,j,k})\, (\boldsymbol{U}_{i+1,j,k} - \boldsymbol{U}_{i,j\,,k})\,.$$

7.2.3. Integration step in the direction y

In the y direction now, the system to solve over a time step Δt is

$$\begin{aligned}
& D_t^y\, \Gamma_{\mathrm{g}} + \partial_y v_{\mathrm{g}} = 0, \\
& D_t^y\, u_{\mathrm{g}} = 0, \\
& D_t^y\, v_{\mathrm{g}} + \partial_y (q(\Gamma_{\mathrm{g}})) = q_g\, \exp(-\Gamma_{\mathrm{g}})\, v_\ell, \\
& D_t^y\, w_{\mathrm{g}} = 0,
\end{aligned}$$

i.e. in vector conservation form

$$D_t^y\, \boldsymbol{U} + \partial_y \mathbf{G} = \mathbf{S}_z.$$

For the discretization, we proceed exactly in the same way as in the integration step in the x direction.

7.2.4. Integration step in the direction z

In the z-direction, the system to solve is

$$\begin{aligned}
& D_t^z\, \Gamma_{\mathrm{g}} + \partial_z w_{\mathrm{g}} = 0, \\
& D_t^z\, u_{\mathrm{g}} = 0, \\
& D_t^z\, v_{\mathrm{g}} = 0, \\
& D_t^z\, w_{\mathrm{g}} + \partial_z (q(\Gamma_{\mathrm{g}})) = -g + q_g\, \exp(-\Gamma_{\mathrm{g}})\, w_\ell.
\end{aligned}$$

For the discretization, we proceed exactly in the same way as in the integration step in the x direction.

7.2.5. Numerical stability of the scheme

Without source terms, the global explicit numerical scheme is conditionally stable according to standard CFL conditions:

$$\frac{\Delta t}{\min(h_x, h_y, h_z)} \max_{(i,j,k)} (c_{i,j,k}) < 1, \tag{25}$$

where $c_{i,j,k}$ denotes the speed of sound of the fluid at mesh point (x_i, y_j, z_k). In real industrial riser reactors, usual fluid velocities are about 10 m/s. That means that the flow is (of course) strongly subsonic with Mach numbers of less than 0.1. Pressure waves then propagate more than 10 times faster than material flow velocity. A consequence is that, due to the CFL constraint (25), more than 10 times step are needed to advance at a characteristic time step of material flow. A trick consists in modifying the equation of state in order to get a flow where the Mach number is of order 0.5, meaning that the material velocity and (artificial) speed of sound are of the same order. This strongly accelerates the time integration and the efficiency of the gas solver. This kind of trick is typically used in smoothed particle hydrodynamics (SPH) computations to artificially raise the numerical Mach number, cf. [13]

7.3. Boundary conditions and embedded geometry conditions

Standard Euler-like boundary conditions are used. At the wall, slip boundary conditions are used, implemented by mirror cells. At the feed inlets, a flow rate is imposed. At the outlet, the pressure is imposed.

Because the true riser cylinder is embedded into a square-base cylinder, for rendering into the actual cylindrical riser column, a kind of extra postprocess at each visualization time step is needed. Actually, we use a smooth function χ such that $\chi \equiv 0$ outside the true cylinder geometry, $\chi \equiv 1$ in the main part of the square-base cylinder, and $0 < \chi(\boldsymbol{x}) < 1$ in a thin subdomain for smooth connection. The gas velocity field, used both for postprocess visualization and as output of the gas model component is

$$\boldsymbol{u}_{\mathrm{g}}(\boldsymbol{x}) \leftarrow \chi(\boldsymbol{x})\, \boldsymbol{u}_{\mathrm{g}}(\boldsymbol{x}). \tag{26}$$

Proceeding like that, one can notice that in particular the gas mean velocity now goes to zero at the true cylinder boundary. That means that slip boundary conditions are transformed into no-slip boundary conditions, as if the gas fluid were viscous.

8. Graphic User Interface, Real Time visualization, interactive simulation

The near Real-Time FCC software was built using open-source cross-platform toolboxes and languages like Python scripting, the powerful visualization toolkit `VTK` [18] with `Python` application programming interface and `wxPython` [20] for high-level widgets and graphic user interface. For efficiency purposes,

critical code like numerical solvers are coded in `C++` and compiled into shared binary libraries. The call of the library function from `Python` is made possible by wrapper utilities like `SWIG` [19].

Figure 1 is an overview of the FCC software during runtime. It is organized as follows:

- a main control window with run, stop and pause buttons. It is also possible to record the flow and user interactions into an AVI video.;
- a graphic user interface that allows us to modify some design parameters and operating conditions like the inlet flow rate, the jet inlet angles, the number of inlets, the ambient temperature;
- a three-dimensional `VTK` window where the geometry and the three phase are rendered in Real Time.

Let us comment the visualization solution. The `VTK` primitives allow us to render the riser reactor column in transparency. Figure 2 shows the rendering of the cylinder skin before running the simulation. `VTK` provides keyboard and mouse interaction to zoom in, zoom out, translate and rotate the cylinder. We

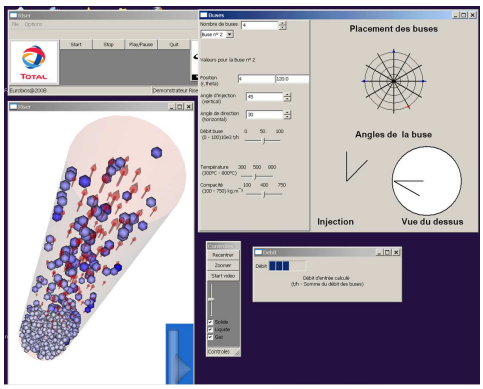

Figure 1: Overview of the near Real-Time FCC software: `VTK`-based visualization window and graphic user interface.

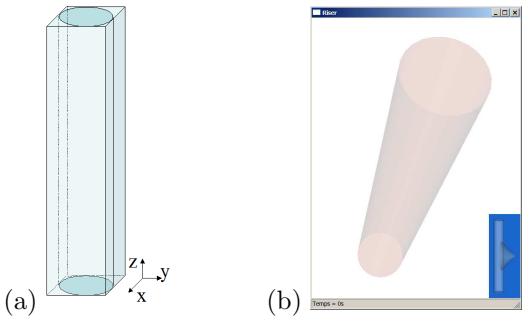

Figure 2: Geometry of riser reactor cylinder: (a) embedded into its square-base cylinder and (b) VTK rendering of the geometry boundary before starting the simulation.

decided to represent the solid catalyst macro-particles as small blue VTK spheres. Because the solid model

is Lagrangian, it is possible to track each particle and compute its residence time into the riser. Then the particles become darker when the residence time becomes big. This is a way to assess the proportion of catalyst fouled up by coke. The liquid oil droplets are represented by green spheres of variables sizes. The size of each sphere follows the evolution of the droplets radius. On figure 3, one can see the liquid oil jets from the feed inlets. The droplets rapidly disappear because of the phase change into gas. Because the gaseous phase is solved by an Eulerian approach, it is no more possible to represent the gas by particles. We used transparent arrows at cell centers. The arrow lengths depend on the velocity magnitude. The arrows move at runtime according to the gas flow, giving a good perception of the turbulence and stable/unstable conditions of the flow.

Numerical experiments were performed on a laptop with a Core 2 Duo Intel CPU and a dual SLI graphic processing unit with hardware acceleration and 2 GB of memory. 300 catalyst macro particles and about 200 liquid droplets were simulated. For the gaseous phase Eulerian solver, a cartesian grid made of $25 \times 25 \times 30$ was used. Real Time was almost reached with reasonable realistic rendering. Due to Moore's law and the evolution of today's multicore technologies that make the parallel computing possible on a standard PC, we think that Real Time could be rapidly reached. On figure 4 we have a view of the riser column and a

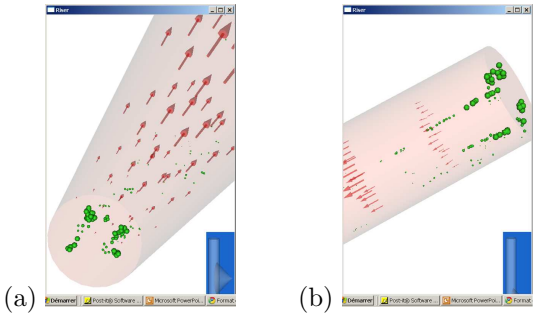

Figure 3: Different views of the flow during simulation: (a) The four crude oil feed inlets with green liquid droplets and red gas velocity arrows; (b) another transversal view of the liquid oil jets.

rendering of the solid catalyst phase. Under the current operating conditions, one can see a privileged solid path emerging near the riser cylinder axis. At the bottom of the cylinder, one can see a strong concentration of solid catalyst particles that form the fluidized bed of the riser reactor. Finally, on Figure 5 we have a snapshot taken during flow exploration from the top of the cylinder. It is possible to dynamically travel through the three dimensional field, select or deselect some phase renderings, zoom, unzoom, rotate, come back to the initial position during runtime.

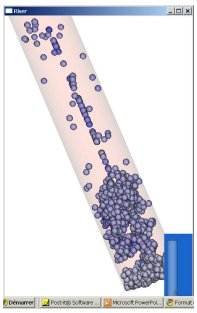

Figure 4: Another view during runtime. The spheres represent the solid macro-particles. We can see an emerging privileged solid path near the axis of the riser cylinder. At the bottom of the cylinder, one can see a strong concentration of solid catalyst particles that form the fluidized bed.

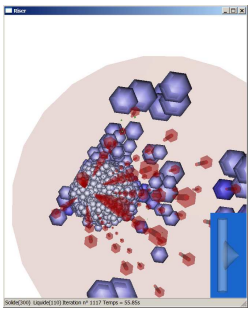

Figure 5: Yet another view from the top into the column. The online interactive visualization allows us to explore and travel into the flow. Solid catalyst particles and gas velocities represented par red arrows are plotted.

9. Concluding remarks

In this paper, we have presented a lightweight physical and numerical model for the near Real Time simulation of FFC flow dynamics into riser reactors columns. Even if the whole model is a rough approximation of the true physics into FCC riser reactors, the model is sufficiently complex to retrieve expected flow features and key features like the turbulence into the fluidized bed, emerging behaviors like the appearance of privileged gas paths, fall down of catalyst particles near walls, phase changes, unstable conditions near contacts between liquid crude oil and catalyst powder, etc... The whole system is actually a full coupled nonlinear system of interacting solid, liquid and gas phase models.

The small number of particles used in the model (a few hundreds) as well as the small resolution of the grid is clearly a problem if one wants to recover more quantitative results, even if significant progress due to new architectures is expected in the near future (cf. [9]). We emphasize that our goal was to provide a tool fulfilling the functional requirements stated in section 3, and not to provide quantitative results for the multiphase flow under study. Among the requirements, we recall that the following features of the flow

had to be recovered (and indeed are recovered): strong gas expansion near crude oil injection, recirculating patterns for catalyst solid phase, privileged paths for the gas phase, strong turbulence in the bottom part of the riser column, laminar regime in the top part, fall down of particles near the riser wall.

The numerical approaches were designed for Computer Graphics and Virtual Reality applications, in order to get near-Real Time capability. For the solid and liquid phases, Lagrangian particles approaches were used. The use of stochastic processes was sufficient to qualitatively represent the turbulence and the diffusion processes. For the leading gaseous phase a standard Eulerian solver and the compressible inviscid fluid perfect gas model were used. To accelerate the numerical solution, a fast solver was designed. It is based on an alternate direction (AD) integration fractional step method. For that, a cartesian grid mesh is necessary. The cylindrical riser column is embedded into the cartesian grid and a smooth cutoff partition function is solved to get the proper boundary conditions onto the true cylindrical geometry.

Of course we do not claim that this model is predictive or even that the numerical results are in agreement with the physics for given operating conditions. But this work has to be seen as a bridge between numerical simulation and virtual reality where numerical simulation can be used as simulator machine for rendering. This is an important issue in the Engineering community for educational or training purposes.

As a result of this work, it was possible to achieve a FCC Real Time software with Real Time three-dimensional visualization rendering and user interaction during runtime. VTK primitives allowed us to design a visualization rendering tool that can visualize solid, liquid and gas phases simultaneously. The solid catalyst particles and liquid crude oil droplets are represented by small moving balls. The gaseous phase flow is represented by velocity arrows that move according to the current velocity flow. The possibility to select or unselect each of the phases and to move into the flow dynamics gives a good perception of what happens into the FCC riser reactor.

[1] R. Krishna, J.M. van Basten, Using CFD for scaling up gas-solid bubbling fluidized bed reactors with Geldart A powders, Chemical Engineering Journal 81 (2001), 247–257.

[2] J. H. Gary and G. E. Handwerk, Petroleum Refining: Technology and Economics (4th Edition ed.), CRC Press (2001), ISBN 0-8247-0482-7.

[3] J. G. Speight, The Chemistry and Technology of Petroleum (4th Edition ed.). CRC Press (2006), ISBN 0-8493-9067-2.

[4] R. Sadeghbeigi, Fluid Catalytic Cracking Handbook (2nd Edition ed.). Gulf Publishing (2000), ISBN 0-88415-289-8.

[5] N. Novia, M. S. Ray and V. Pareel, Three-dimensional hydrodynamics and reaction kinetics analysis in FCC Riser reactors, Chemical product and process modeling, Vol. 2, issue 2 (2007).

[6] S. Benyahnia, H. Arastoopour, T. M. Knowlton and H. Massah, Simulation of particles and gas flow behavior in the riser section of a circulating fluidized bed using the kinetic theory approach for the particulate phase, Powder Technology, 112 (2000), 24–3.

[7] S. Benyahnia, A. G. Ortiz, and J.I.P. Paredes, Numerical analysis of a reacting gas/solid in the riser section of an industrial fluid catalytic cracking unit, International Journal of Chemical reactor engineering, 1 (2003), 1–11.

[8] J. S. Ahari, A. Farshi and K. Forsat, A mathematical modeling of the riser reactor in industrial FCC unit, Petroleum and Coal, 50(2) (2008), 15–24.

[9] F. De Vuyst, F. Salvarani,GPU-accelerated numerical simulations of the Knudsen gas on time-dependent domains, Comput. Phys. Comm., 184, 3 (2013) 532-536.

[10] J. F. Parmentier, O. Simonin and O. Delsart, A numerical study of fluidization behaviour of Geldart B, A/B and A particles using an Eulerian multifluid modeling approach, in: Circulating Fluidized Bed Technology IX, Hamburg, Germany (2008).

[11] G. N. Ahuja and A. W. Patwardhan, CFD and experimental studies of solid hold-up distribution ans circulation patterns in gas-solid fluidized beds, Chemical Engineering Journal, 143 (2008), 147–160.

[12] R. C. McFarlane, R. C. Reineman, J. F. Bartee and C. Georgakis, Dynamic simulator for a model IV Fluid Catalytic Cracking Unit, Computers & Chemical engineering, vol. 17, 3 (1993), 275–300.

[13] J.J. Monaghan, Simulating free surface flows with SPH, J. Comp. Phys., 11:225-235 (1994).

[14] J. S. Halow, C. S. Daw and C.E. Finney, Emergent behaviour in a low-order fluidized bed bubble model, AIChE Annual meeting, LA, CA (2000), paper 15, URL `http://www-chaos.engr.utk.edu/pap/aiche2000halow-paper.pdf`.

[15] S. Pannala, C. S. Daw and J. S. Halow, Simulations of reacting fluidized beds using an agent-based bubble model, Int. Journal of Chemical Reactor Engineering, Vol. 1, Article A20 (2003).

[16] Pannala, S., C. S. Daw and J. S. Halow, Near Real-time Simulations of Large Fluidized Beds with a Low Order Bubble Model, Session 199b, AIChE Annual Meeting, Reno, Nevada, November 4-9, (2001).

[17] M. Ye, M. A. van der Hoef and J.A.M. Kuipers, A numerical study of fluidization behavior of Geldart A particles using a discrete particle model, Powder technology, 139 (2004), 129–139.

[18] VTK, the visualization toolkit, `http://www.vtk.org`.

[19] SWIG, simplified wrapper and interface generator, `http://www.swig.org`.

[20] wxWidgets, cross-platform GUI library, `http://www.wxwidgets.org` and `http://www.wxpython.org`